

Article

# Effect of Modification with Different Contents of Sb and Sr on the Thermal Conductivity of Hypoeutectic Al-Si Alloy

Jin Guo, Zhi-Ping Guan, Rui-Fang Yan, Pin-Kui Ma, Ming-Hui Wang, Po Zhao and Jin-Guo Wang \*

Key Laboratory of Automobile Materials of Ministry of Education & School of Materials Science and Engineering, Nanling Campus, Jilin University, No. 5988 Renmin Street, Changchun 130025, China; kwokking@outlook.com (J.G.); guanzp@jlu.edu.cn (Z.-P.G.); yanruifang@jlu.edu.cn (R.-F.Y.); mapk@jlu.edu.cn (P.-K.M.); minghui@jlu.edu.cn (M.-H.W.); zhaopo@jlu.edu.cn (P.Z.)

\* Correspondence: jgwang@jlu.edu.cn; Tel.: +86-431-8509-4699

Received: 12 October 2020; Accepted: 3 December 2020; Published: 5 December 2020



**Abstract:** In this paper, the effects of size, morphology and distribution of eutectic silicon on the thermal conductivity of Al-8Si alloy modified by Sr (0.04, 0.08, 0.12 wt.%) and Sb (0.1, 0.3, 0.5 wt.%) elements with T6 heat treatment were investigated. The results show that the modified fibrous eutectic silicon has a significant capability of improvement of thermal conductivity, while the amount of the modifier has a relatively weak effect on thermal conductivity. After T6 treatment, the fracture or spheroidization of the flake eutectic silicon and the disappearance of clustering phenomenon could raise thermal conductivity, but the coarsening of fibrous eutectic silicon is inconducive to thermal conductivity. Finally, the effect of eutectic silicon on electron transport is analyzed in detail, which could provide a reference for enhancing the thermal (or electrical) conductivity of hypoeutectic Al-Si alloy through effective microstructure control.

**Keywords:** Al-Si alloy; modification; eutectic silicon; thermal conductivity; heat treatment

## 1. Introduction

Most of aluminum alloy castings are aluminum–silicon alloy [1]. Al-Si alloy is widely applied in automobile, aviation, electrical and communication industries because of its good casting performance, low density, low cost, good electrical conductivity, thermal conductivity and mechanical properties [2–4]. With the development of communication technology recently, the communication base stations are springing up all over the world, where the heat dissipation performance of the radiator is a vital important index for the work efficiency of communication electrical components. Because the radiators in base station mainly are fabricated by aluminum–silicon alloy, its thermal conductivity has been a significant issue [5], and the improvement of the thermal conductivity of Al-Si alloy is of theoretical significance for material science and practical value for communication station.

Some research on the thermal conductivity and electrical conductivity of aluminum alloys has proved that there is a linear correlation between thermal conductivity and electrical conductivity [6]. Boron treatment is one of the methods to enhance electrical and thermal conductivity. The impurity elements in the melt reduce the electrical conductivity of the alloy, and the electrical conductivity can be increased after the boron treatment [7–9]. Adding trace Ti can improve the treatment effect of boron treatment and promote the transformation of impurity elements from solid solution state to precipitation in the form of compounds, thus improving the electrical conductivity [10]. With regard to the research on the improvement of electrical conductivity by modification, the main point of view is that the morphology of eutectic silicon changes after modification, and electrons pass through

the eutectic region more easily, thus improving the electrical conductivity [11–13]. Heat treatment is also a common means of microstructure control. Solution treatment refines and spheroidizes eutectic silicon and reduces the number of second phases. The aging treatment can precipitate fine precipitates, thus improving the thermal conductivity [14]. The solution temperature and solution time have influences on microstructure change. With the increase of solution time, eutectic silicon will go through three stages: fracture, spheroidization and growth coarsening. After aging treatment, the precipitation of intermetallic compounds consumes the solute elements originally dissolved in the matrix, which raises thermal/electrical conductivity [15–17]. In addition, the type of modification and cooling rate could affect the distribution of porosity and then affect electron propagation, resulting in changes in thermal conductivity [18].

In summary, the effect of different sizes and morphologies of eutectic silicon on thermal/electrical conductivity of the alloy needs to be investigated. Since some investigations show that Na, Sr [19], Eu [20], Ba [21] and Y [22] can modify eutectic silicon in fibrous shape, and Sb and Bi can modify eutectic silicon in fine flake shape [23], the addition of alloy elements can affect the eutectic morphology of the alloy [24]. In the study, the eutectic morphology of Al-8Si alloy would be controlled through the addition of elements Sr and Sb, in order to investigate the effect of the size and morphology of eutectic silicon of the alloy. Through combining T6 heat treatment, in addition, the size and shape of eutectic silicon of the alloy would be furtherly changed. Then, the dependency of thermal/electrical conductivity on different sizes and morphologies of eutectic silicon of Al-8Si alloy would be investigated. Finally, it is aimed to get fine fibrous/flake shape eutectic silicon of Al-8Si alloy which is beneficial to its thermal/electrical conductivity.

## 2. Materials and Methods

In this work, a resistance furnace (SG2-7-12, Shanghai, China) with a rated power of 5 kW and a rated temperature of 1200 °C was used to melt the alloy. In order to prevent extra impurity elements from entering the melt, the surface of the tools used should be coated with ZnO and dried. Al-8Si (wt.%, unless otherwise stated, use throughout the paper) was prepared from pure Al and Al-24.4Si master alloys. Firstly, pure Al (99.8%) and Al-24.4Si master alloy were put into a graphite crucible and heated to 780 °C in a resistance furnace. When the alloy began to melt, the temperature was adjusted to 750 °C. After the alloy was completely melted, the impurities floating on the melt were removed and held for 5 min. Then, the preheated Al-10Sr alloy coated in aluminum foil was added into the melt (in this step, when Sb was used for modification, Al-10Sr was replaced by pure Sb), and the melt was fully stirred and kept for 15 min. Finally, degassing with argon for 2 min. After skimming off the dross, the melts with different kinds and contents of modifiers were poured into the cast steel mold preheated to 200 °C in advance to get Al-8Si-xSr and Al-8Si-xSb alloys.

The chemical composition of each sample was measured with optical spectrum analyzer (ARL 4460, Ecublens, Switzerland), and at least four points were measured, and the average value of each sample was calculated. Table 1 shows the chemical composition of the alloys. After modification, fibrous and flake eutectic silicon can be obtained. In order to obtain spherical eutectic silicon, the samples need to be cut from the modified alloys for T6 heat treatment, were solid solution was treated at 535 °C for 4 h, then water quenching to 25 °C, finally artificial aging at 170 °C for 3 h.

The samples were polished by standard procedure, then deeply etched in 5 vol.% HF solution and then examined by scanning electron microscopy (SEM) (Zeiss Evo 18, Zeiss, Oberkochen, Germany) equipped with energy dispersive spectrometer (EDS). Because the color of Al matrix is similar to that of eutectic Si and the size of fibrous eutectic Si is small, in order to ensure the accuracy of measurement, Nano Measurer1.2 software (1.2.5, Fudan University, Shanghai, China) is selected to measure the size of eutectic silicon. Ten images were selected for each sample, and the sizes of more than 20,000 eutectic silicon phases were measured. Because a large amount of fine fibrous eutectic silicon is very round, only the width of fibrous eutectic silicon is measured.

**Table 1.** Chemical compositions of Al-8Si alloys (wt.%).

Alloy	Si	Fe	Cu	Mg	Mn	Ti	Sb	Sr	Al
Al-8Si	8.06	0.20	0.004	0.001	0.004	0.002	-	-	Bal.
Al-8Si-0.1Sb	7.85	0.22	0.004	0.002	0.005	0.002	0.09	-	Bal.
Al-8Si-0.3Sb	7.82	0.21	0.004	0.001	0.003	0.001	0.27	-	Bal.
Al-8Si-0.5Sb	7.85	0.21	0.004	0.001	0.003	0.002	0.46	-	Bal.
Al-8Si-0.04Sr	8.04	0.21	0.004	0.001	0.003	0.001	-	0.033	Bal.
Al-8Si-0.08Sr	7.98	0.22	0.004	0.001	0.003	0.001	-	0.072	Bal.
Al-8Si-1.2Sr	8.09	0.23	0.004	0.001	0.003	0.001	-	0.108	Bal.

The heat transfer of metals mainly relies on free electrons, and there is an inevitable connection between electrical conductivity and thermal conductivity, which can be connected by the Wiedemann–Franz law:

$$\lambda = LT\sigma, \quad (1)$$

where  $\lambda$  is the thermal conductivity,  $\sigma$  is the electrical conductivity,  $T$  is the temperature,  $L$  Lorentz number. For aluminum alloy,  $L$  is  $2.1 \times 10^{-8} \text{ W}\Omega\text{K}^{-2}$  [25]. In aluminum alloy containing Si,  $L$  increases with the increase of Si content,  $L$  is  $2.1 \times 10^{-8} + 0.021 \times 10^{-8} \times \text{wt.\% Si W}\Omega\text{K}^{-2}$  [26]. For aluminum alloy, Wiedemann–Franz law is modified

$$\lambda = LT\sigma + c, \quad (2)$$

where  $c$  is  $12.6 \text{ W}/(\text{m}\cdot\text{K})$  [25–27]. For hypoeutectic alloys, under the measurement conditions from  $20^\circ\text{C}$  to  $60^\circ\text{C}$ , in accordance with the modified Wiedemann–Franz law, there is a linear correlation between the calculated thermal conductivity and the measured value [6]. The electrical conductivity of the alloy was measured by electrical conductivity measuring instruments (Sigmatest 2.069, Foerster, Reutlingen, Germany) at room temperature. Eight data were measured for each sample, and the measured results were converted into % IACS, and the average value was calculated. The thermal conductivity is obtained by the modified Wiedemann–Franz law.

### 3. Results

#### 3.1. Microstructure

The SEM photographs of the alloys before and after modification are shown in Figure 1. In Figure 1a, unmodified eutectic silicon appears a typical flake morphology. Eutectic silicon grows on  $\alpha$ -Al as the leading phase, and then eutectic aluminum nucleates on the leading nucleation eutectic silicon and then grows into eutectic structure. The microstructures of Al-8Si alloy modified by different contents of Sb are as shown by Figure 1b–d. Figure 1b shows that, compared with Figure 1a, the eutectic silicon begins to become finer and distributes regularly after adding 0.1 wt.% Sb. With the addition of 0.3 wt.% Sb, the proportion of finer eutectic silicon increases. It is worth noting that the distribution of eutectic silicon has been significantly changed. The eutectic silicon will aggregate at a certain angle and direction, showing a cluster morphology, as shown in Figure 1c. After adding 0.5 wt.% Sb, the proportion of fine eutectic silicon is further increased, and the clustering phenomenon is more obvious, as shown in Figure 1d. The results show that as the content of Sb increases, fine eutectic silicon will increase, the clustering phenomenon will be more obvious, and the distribution of eutectic silicon will become more uneven. It can be seen from figures Figure 1e–g that eutectic silicon has been changed from flake shape to fibrous shape with the addition of Sr. Compared with the unmodified eutectic silicon in Figure 1a, the size of the eutectic silicon greatly decreases. The morphology and distribution of eutectic silicon have no obvious change with the increase of Sr content.

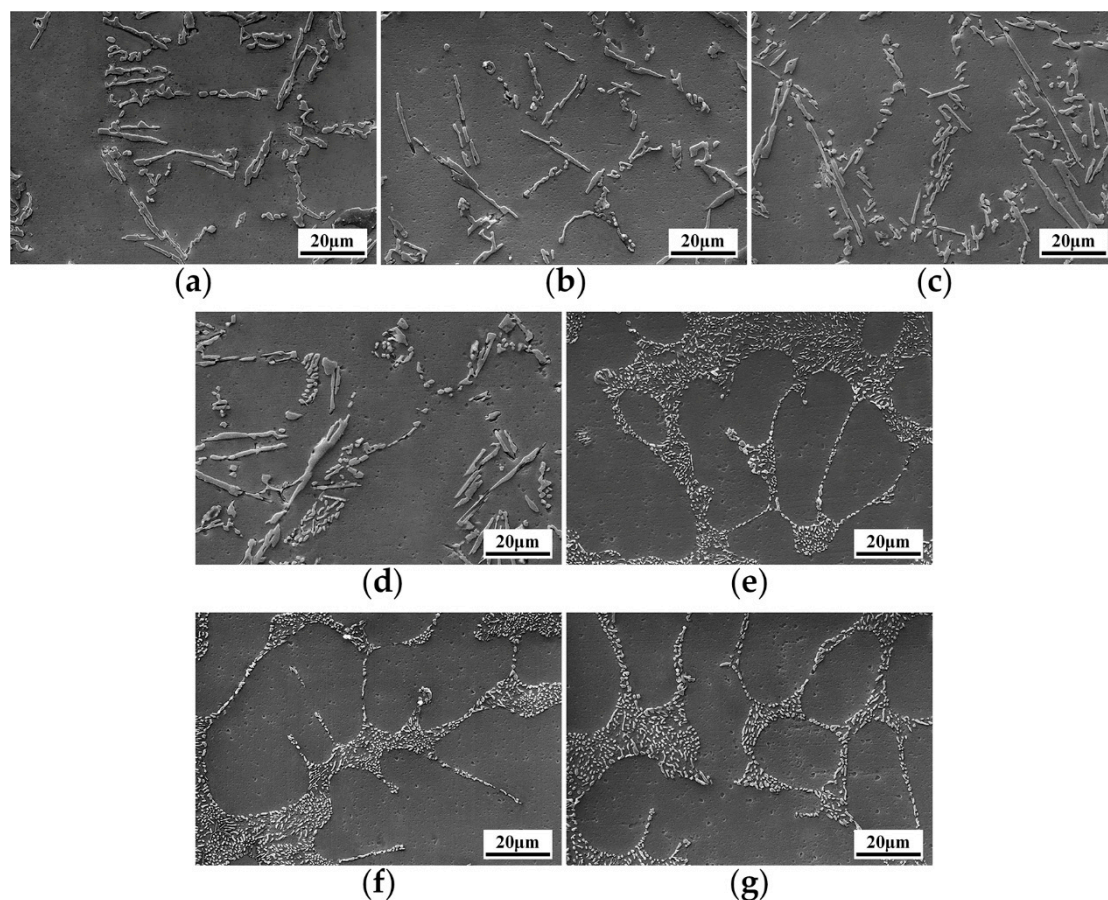


**Figure 1.** SEM microstructure of eutectic silicon in Al-8Si alloys with different contents of modifiers: (a) unmodified, (b) 0.1 wt.% Sb, (c) 0.3 wt.% Sb, (d) 0.5 wt.% Sb, (e) 0.04 wt.% Sr, (f) 0.08 wt.% Sr, (g) 0.12 wt.% Sr.

Through statistics analysis of eutectic silicon size before and after modification, the data are summarized as shown in Figure 2. The error bar in this paper is calculated from the standard deviation (S.D.), which reflects the degree of discreteness of the value relative to the average value. Figure 2a,b shows that the average length and width of unmodified eutectic silicon are  $\sim 9.80 \mu\text{m}$  and  $\sim 2.56 \mu\text{m}$ , respectively. With the increase of Sb content, the average length and width of eutectic silicon decrease, but when 0.5 wt.% Sb is added, the length and width increase slightly to  $\sim 9.61 \mu\text{m}$  and  $\sim 1.92 \mu\text{m}$ , respectively, indicating excessive modification. Moreover, it can be seen from Figure 1b-d that a large number of fine flake and long flake eutectic silicon coexist. It is worth noting that, the size distribution of eutectic silicon, combined with Figure 2d,e, also confirms the above rule. As shown in Figure 2c, when the content of Sr is 0.04 wt.%, 0.08 wt.% and 0.12 wt.%, the average width of eutectic silicon is  $\sim 0.94 \mu\text{m}$ ,  $\sim 0.76 \mu\text{m}$  and  $\sim 0.65 \mu\text{m}$ , respectively. It can be seen that the size of fibrous eutectic silicon gradually decreases with the increase of Sr content. In Figure 2f, compared with unmodified eutectic silicon, the size distribution of eutectic silicon modified by Sr is more concentrated with a normal distribution.

The microstructures of the alloy after T6 heat treatment are shown in Figure 3. Al-8Si alloy is modified by Sb and Sr to obtain fine flake and fibrous eutectic silicon. Spherical eutectic silicon can be obtained after T6 heat treatment, especially in the solid solution treatment stage, and the silicon phases break, spheroidize and grow, and the aspect ratio of silicon phase is increased [16,28]. Therefore, for the unmodified eutectic silicon in Figure 3a and the Sb modified eutectic silicon in Figure 3b–d after the T6 heat treatment, the long flake eutectic silicon is fractured or even spheroidized. However, after T6 heat treatment, the fibrous eutectic silicon modified by Sr is spheroidized, coarsening and growing up, such as the coarsening spherical eutectic silicon in Figure 3e–g.

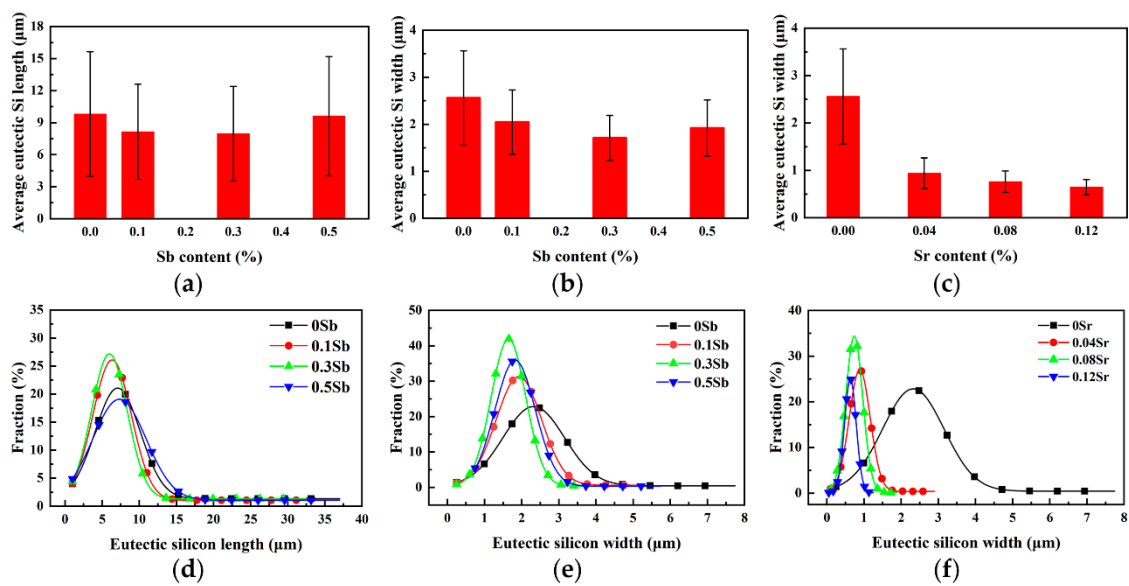


**Figure 2.** Distribution and variation of eutectic silicon size in Al-8Si alloys with the addition of different modifiers: (a) variation of length after Sb modified, (b) variation of width after Sb modified, (c) variation of width after Sr modified, (d,e) distribution of size after Sb modified, (f) distribution of size after Sr modified.

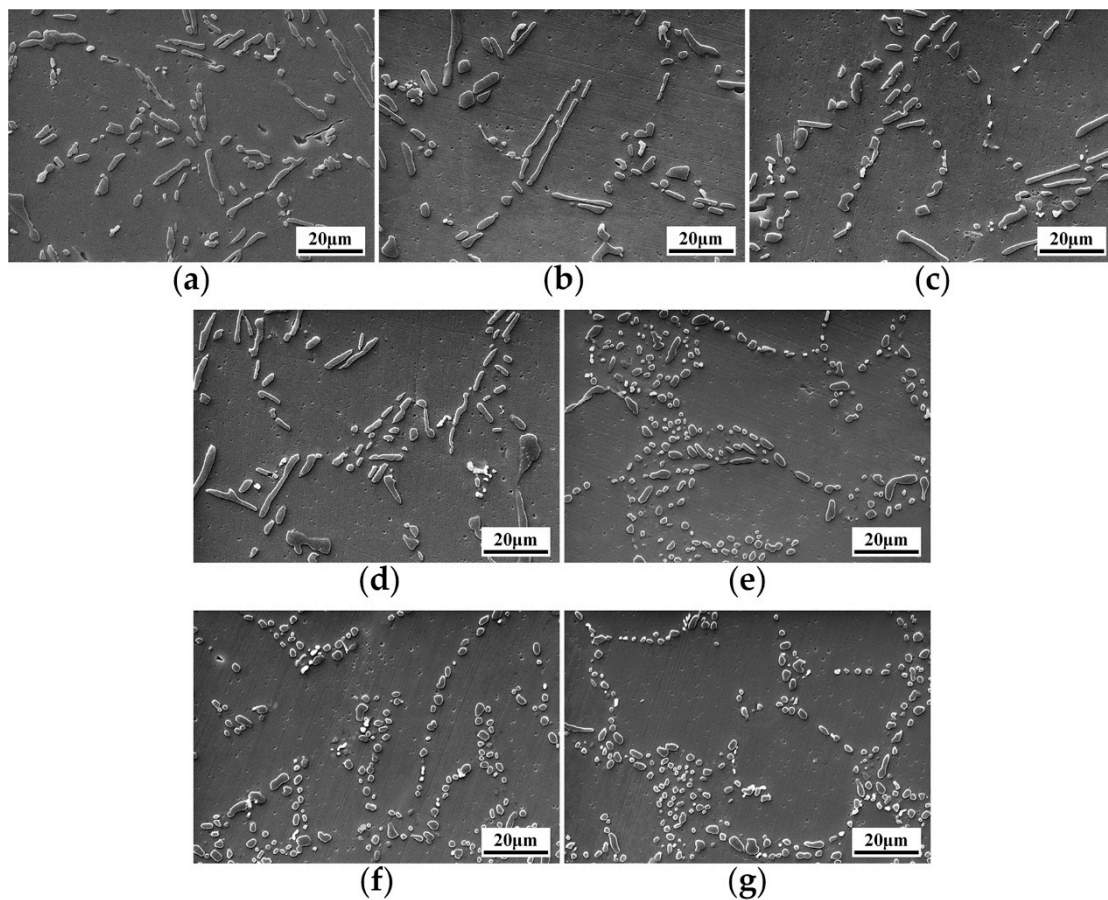


**Figure 3.** SEM microstructure of eutectic silicon in Al-8Si alloys with different contents of modifiers after T6 heat treatment: (a) unmodified + T6, (b) 0.1 wt.% Sb + T6, (c) 0.3 wt.% Sb + T6, (d) 0.5 wt.% Sb + T6, (e) 0.04 wt.% Sr + T6, (f) 0.08 wt.% Sr + T6, (g) 0.12 wt.% Sr + T6.

Figure 4 shows after T6 heat treatment the size change and distribution of eutectic silicon. It can be seen from the Figure 4a,b that the size of eutectic silicon modified by Sb is close to that without modification. The average length and width of eutectic silicon with 0.5 wt.% Sb content are  $\sim 7.11 \mu\text{m}$  and  $\sim 1.73 \mu\text{m}$ , respectively. It can be seen from Figure 4d,e that the size distribution of unmodified eutectic silicon is similar to that of Sb modified eutectic silicon after T6 heat treatment. It is worth noted that after T6 heat treatment, the eutectic silicon modified by Sr is much coarser than its as-cast size, and the average width of 0.08 wt.% Sr content has reached  $1.80 \mu\text{m}$ , while the corresponding average width of as-cast is only  $\sim 0.76 \mu\text{m}$ . In addition, with different Sr content, the average size distribution of eutectic silicon is relatively concentrated but still presents a normal distribution. This indicates that although the overall size of eutectic silicon is coarsened after spheroidization, the size distribution is relatively uniform, as shown in Figure 4c,f.

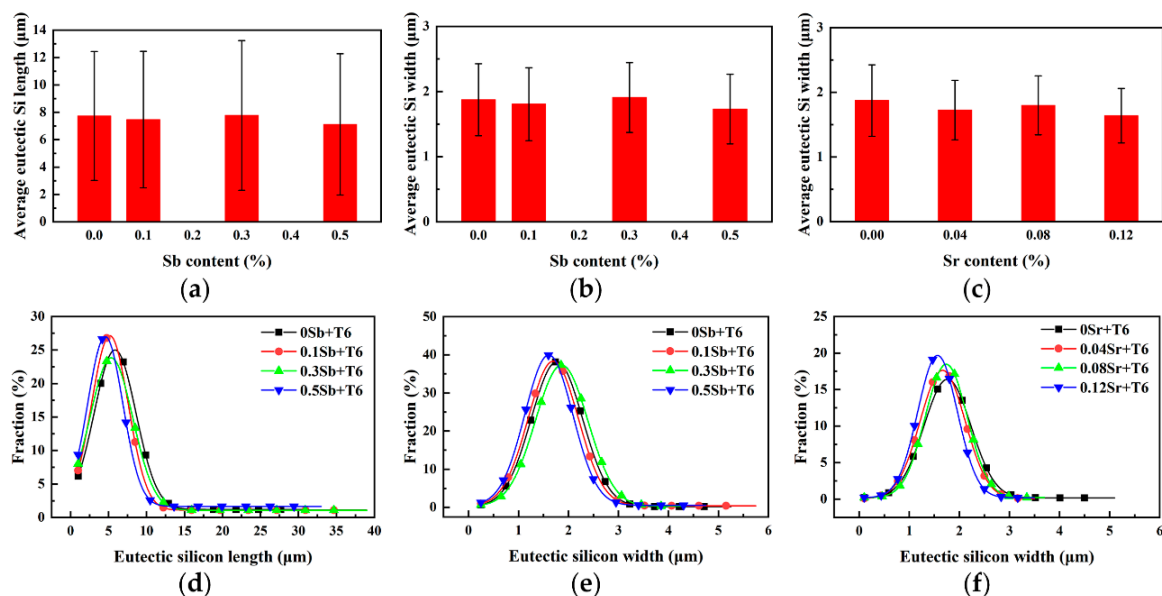


**Figure 4.** Distribution and variation of eutectic silicon size in Al-8Si alloys with the addition of different modifiers after T6 heat treatment: (a) variation of length after Sb modified, (b) variation of width after Sb modified, (c) variation of width after Sr modified, (d,e) distribution of size after Sb modified, (f) distribution of size after Sr modified.

In general, eutectic silicon presents flakes after Sb modification and short flakes after T6 treatment, so these two states are called flake shape. Eutectic silicon is fibrous after Sr modification and becomes spheroidizing and coarsening after T6 treatment. These two states are called granular shape, and from statistical data, it can be seen that the overall size of granular eutectic silicon is obviously smaller than that of flake eutectic silicon.

The size and distribution of eutectic silicon have an impact on thermal/electrical conductivity of the alloy. In addition to Al and Si, the alloy in this work also contains impurity element Fe and modification elements Sb and Sr. The SEM and EDS of Al-8Si alloy in different states are shown in Figure 5. From Figure 5e–h, Si exists in the form of eutectic silicon phase of the alloy. As an impurity element in Al-Si alloys, generally, Fe often exists in different forms of intermetallic compounds [29]. Sb is evenly distributed in the matrix and exists with solid solution. Sr element changes the growth of eutectic silicon by adsorbing on eutectic silicon [30,31].

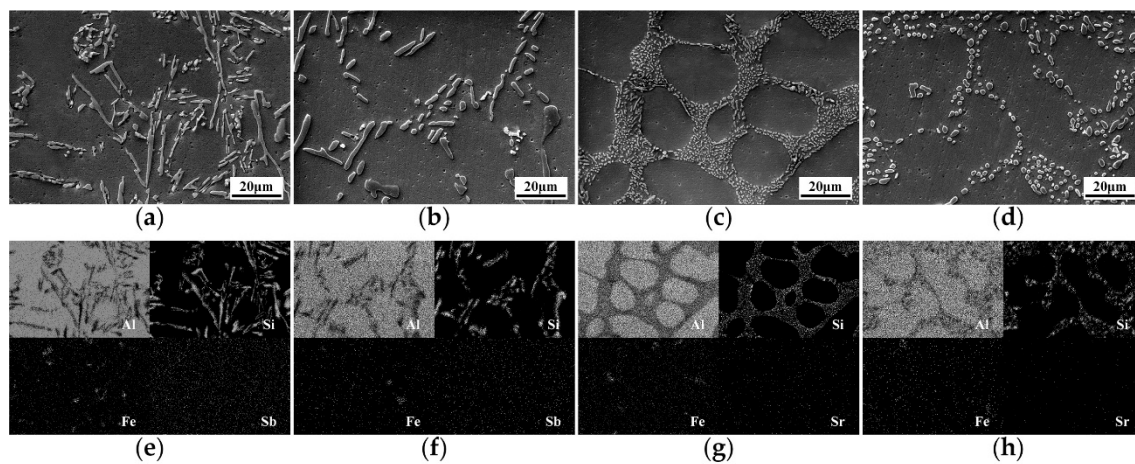


**Figure 5.** (a–d) Scanning electron microscope (SEM) micrographs and (e–h) energy dispersive spectrometry (EDS) of Al-8Si alloys in different states: (a) 0.5 wt.% Sb, (b) 0.5 wt.% Sb + T6, (c) 0.12 wt.% Sr, (d) 0.12 wt.% Sr + T6, (e–h) corresponding EDS mapping images of (a–d).

### 3.2. Thermal and Electrical Conductivities

The changes of electrical/thermal conductivity of Al-8Si alloy after modification and T6 heat treatment are shown in Figure 6. Table 2 shows the electrical/thermal conductivity of Al-8Si alloy in different states and eutectic silicon size and morphology. The average size is half the sum of the average length and the average width. In Figure 6a, the thermal/electrical conductivity of the alloy is enhanced through 0.1 wt.% Sb modification, but when the Sb content comes to 0.3 wt.% and 0.5 wt.%, the thermal/electrical conductivity begins to decrease. Combined with Figures 1 and 2, it can be seen that after 0.1 wt.% Sb modification, the average length and width of eutectic silicon are reduced, the electron channels are increased, and the mean free path is increased, so the electrical conductivity is improved. When the Sb content further comes to 0.3 wt.% and 0.5 wt.%, on the one hand, fine eutectic silicon and flake eutectic silicon coexist, resulting in an increase in aspect ratio; on the other hand, eutectic silicon has directional aggregation and clustering phenomenon, which results in the decrease of electron channels and the increase of electron scattering, so that the thermal and electrical conductivities begin to decline or even lower than that of unmodified eutectic silicon. However, as the Sr content goes up, the electrical conductivity of the alloy increase slightly. Combined with Figures 1 and 2, the size of fibrous eutectic silicon modified by Sr is very small and has little difference, but compared with that without modification, the electronic channel increases greatly, and the thermal and electrical conductivities increase a lot.

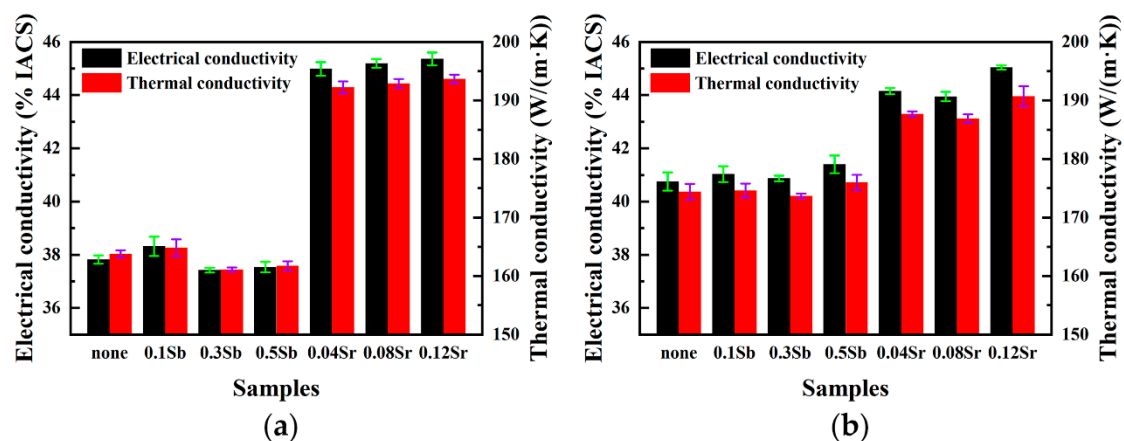


**Figure 6.** Electrical and thermal conductivities of Al-8Si alloys in different states: (a) electrical and thermal conductivity of as-cast alloys, (b) electrical and thermal conductivity of T6 state alloys.

**Table 2.** The eutectic silicon characteristics, measured electrical ( $\sigma$ ) conductivity, temperature (T) and calculated thermal ( $\lambda$ ) conductivity values of the alloys.

Sample State	Average Length ( $\mu\text{m}$ )	Average Width ( $\mu\text{m}$ )	Average Size ( $\mu\text{m}$ )	Aspect Ratio	$\sigma$ (% IACS)	T ( $^{\circ}\text{C}$ )	$\lambda$ (W/(m·K))
Unmodified	9.81	2.56	6.19	3.83	37.8	29.9	163.8
0.1Sb	8.14	2.04	5.09	3.98	38.3	29.9	164.9
0.3Sb	7.96	1.71	4.84	4.65	37.4	29.9	161.1
0.5Sb	9.61	1.92	5.77	5.01	37.5	29.9	161.7
Unmodified + T6	7.73	1.87	4.80	4.13	40.8	27.9	174.4
0.1Sb + T6	7.47	1.81	4.64	4.14	41.0	27.9	174.6
0.3Sb + T6	7.78	1.91	4.85	4.07	40.9	27.9	173.7
0.5Sb + T6	7.11	1.73	4.42	4.11	41.4	27.9	175.0
0.04Sr	-	0.94	-	-	45.0	29.9	192.3
0.08Sr	-	0.76	-	-	45.2	29.9	192.9
0.12Sr	-	0.65	-	-	45.4	29.9	193.7
0.04Sr + T6	-	1.73	-	-	44.2	27.9	187.7
0.08Sr + T6	-	1.80	-	-	43.9	27.9	186.9
0.12Sr + T6	-	1.64	-	-	45.0	27.9	190.7

It can be seen from Figure 6b that after T6 heat treatment, the properties of Sb modified are almost the same as those without modification. It is worth noting that the performance of 0.5 wt.% Sb modification is the highest at this time, because on the one hand, there are many fine eutectic silicon before heat treatment, and the longer eutectic silicon also breaks after heat treatment, so that the size of eutectic silicon decreases, and the clustering phenomenon disappears. On the other hand, the aspect ratio is also the lowest. This makes the performance of 0.5 wt.% Sb modification the best. Combined with Figures 3 and 4, because the size of fibrous eutectic silicon modified by Sr is very small, spheroidizing and coarsening occurs after T6 treatment, so that the number of eutectic silicon in the limited area decreases, that is, the number of electron channels is reduced, so the properties are lower than those before heat treatment. In general, the thermal and electrical conductivities are greatly affected by the distribution, size and morphology of eutectic silicon. Sb modification has little effect on the morphology of eutectic silicon, which is still flake morphology, and the eutectic silicon cluster distribution appears when the Sb content continues to increase, and the average size is not much different, so there is little difference in as-cast thermal/electrical conductivity. Although the morphology of eutectic silicon only changes partially after T6 treatment, the average size and aspect ratio decrease; as well as the disappearance of clustering phenomenon, all make the thermal/electrical conductivity of T6 improved compared with as-cast. After Sr modification, the size of eutectic silicon is relatively small, and the size distribution is normal distribution. The size of eutectic silicon increases after heat treatment, and the thermal/electrical conductivities are lower than that of as-cast, but the thermal and electrical conductivities are still much higher than those of unmodified eutectic silicon. It can be seen that granular (fibrous and spherical) eutectic silicon is smaller and more dispersed than flake eutectic silicon, which is more conducive to the transmission of electrons.

#### 4. Discussion

It can be explained from the theory of impurity-induced twinning (IIT) [32] that eutectic silicon presents fibrous morphology after Sr modification. Sr is adsorbed in the eutectic silicon step [33,34], which makes it impossible for Si atoms to grow into flakes. In addition, Sr atoms adsorbed on eutectic silicon change the stacking order of Si atoms. Eutectic silicon grows into a fibrous shape by the twin plane re-entrant edge mechanism (TPRE) [35]. After Sb is added to the Al-Si alloy, Sb and Al combine to form an AlSb phase [36]. In addition, there are Sb atoms dissolved in the matrix. These AlSb phases or Sb clusters are preferentially adsorbed and enriched at the front of the eutectic silicon growth interface [37], resulting in a decrease in the size of eutectic silicon and the formation of fine flake eutectic silicon with local aggregation in a certain angle and direction. Regarding the solution treatment in the T6 heat treatment, the eutectic silicon in the modified alloy has begun to fuse within 30 min and then begins to spheroidize and grow coarsening, which explains that the fibrous eutectic silicon

modified by Sr is coarsening spherical after heat treatment in this article, while the eutectic silicon in the unmodified alloy continues to fuse after 4 h, which will make the fine eutectic silicon melt, spheroidize and even grow up. The long flake eutectic silicon continues to fuse, which can explain that the clustering phenomenon of the Sb modified alloy mentioned above disappears after heat treatment, overall size and aspect ratio of the eutectic silicon decrease [16,17]. In addition, during the aging treatment process, the solute elements in the matrix are reduced, and intermetallic compounds are precipitated, which improves the thermal conductivity of the alloy [15].

To better illustrate the effect of the morphology and size of eutectic silicon before and after modification and heat treatment on the thermal and electrical conductivities of the alloy, the schematic diagram shown in Figure 7 is made [2,12]. From Figure 7a, it can be seen that the unmodified eutectic silicon is long flake, on the one hand, Si is a semiconductor, so the collision between electron and Si results in electron scattering [2]; on the other hand, the Al matrix is a conductor, and electrons are transmitted in the matrix, so the coarse eutectic silicon will cause electron scattering. Figure 7d shows the unmodified eutectic silicon after T6. It can be observed that the coarse silicon phase breaks, which increases the electron channel and the mean free path of the electron, so the electrical conductivity is improved. The eutectic silicon is modified by Sb, as shown in Figure 7b; although there are many fine Si phases, there is still a long eutectic silicon, and the eutectic silicon has clustering phenomenon, which leads to the increase of electron scattering and the decrease of the mean free path. This explains that the thermal and electrical conductivities of 0.3 wt.% Sb and 0.5 wt.% Sb modified alloys are even lower than that of the unmodified alloy. Figure 7e is the case after T6 heat treatment; the longer eutectic silicon breaks, and the locally aggregated eutectic silicon is refined, so the electron channel increases, and the mean free path increases obviously, so the electrical conductivity of the alloy is also enhanced. As shown in Figure 7c, eutectic silicon modified by Sr becomes very fine fibrous. At this time, the electron channel increases greatly; the collision probability between electron and Si phase decreases; the electron scattering decreases, and the mean free path increases greatly, which makes the alloy conductivity of fibrous eutectic silicon the highest in this experiment. Combined with Figure 7f, it can be seen that although the fibrous eutectic silicon is spheroidized after T6 treatment, it is also coarsened at the same time. From the marked red circle, it can be seen that in the same size area, the coarser spheroidized eutectic silicon will reduce the electron channel, so its electrical conductivity is not as good as the fiber before heat treatment, which is determined by the heat treatment parameters of this experiment. The eutectic silicon with spheroidization but not coarsening should be obtained by properly reducing the heat treatment temperature and time (for example, within the 30 min mentioned above). The research in this aspect is also worth exploring.

For the alloy containing trace Mn [38], the size, quantity and morphology of Fe phase change little during T6 heat treatment, and the addition of Fe has little effect on Si particles [39]. The content of the impurity element Fe is almost the same in this experiment, and its influence on the electrical and thermal conductivities of the alloy is very weak. According to Matthiessen's rule, defects increase the resistivity of metal materials, and the expression is as follows:

$$\rho_{\text{total}} = \rho_t + \rho_i + \rho_d, \quad (3)$$

where  $\rho_{\text{total}}$  is the total resistivity, and  $\rho_t$ ,  $\rho_i$  and  $\rho_d$  are the resistivity caused by thermal vibration, impurities and lattice defects, respectively [40]. For pure Al, the solid solution of atoms contained in  $\rho_d$  has the greatest contribution to the total resistivity [40,41], and because the modification element Sb has almost no adverse effect on the electrical conductivity of 99.99% aluminum [42], it can be explained that the part of Sb atoms dissolved in the matrix has little effect on the electrical conductivity of the alloy, which is consistent with the experimental results, and the clustering phenomenon of 0.5 wt.% Sb modification after T6 heat treatment disappears. The electrical conductivity of the alloy is higher than that of the unmodified alloy. However, the Sr atom is attached to the Si phase, so there is almost no Sr solid solution in the matrix. It can be concluded that the modification changes the morphology of eutectic silicon, and the relatively fine eutectic silicon has better thermal and electrical conductivities

under the premise of little difference in eutectic silicon distribution. T6 heat treatment not only fuses the long and thick eutectic silicon but also makes the fine eutectic silicon spheroidize or even coarse. The effect of heat treatment time and temperature on it is also worth exploring.

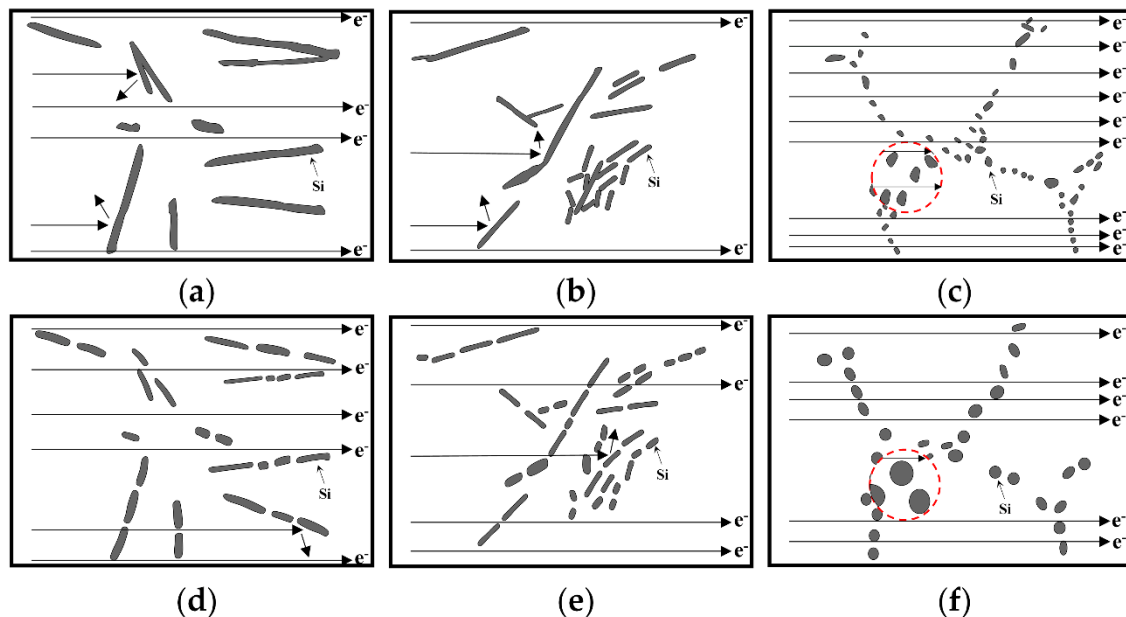


**Figure 7.** Schematic diagram of electron collision with eutectic silicon and electron transfer: (a) unmodified, (b) Sb modification, (c) Sr modification, (d) unmodified + T6, (e) Sb modification + T6, (f) Sr modification + T6.

In general, the improvement of the thermal and electrical conductivities of the alloy is limited when there is no significant change in the morphology and size of the modified eutectic silicon compared with the unmodified eutectic silicon. However, when the alloy is modified to spherical and fibrous, the thermal and electrical conductivities of the alloy are greatly enhanced. According to the actual conditions and environment, eutectic silicon with different sizes and morphologies can be obtained by modification and heat treatment, so that relatively accurate microstructure control and improvement of thermal and electrical conductivities can be achieved by adjusting and optimizing casting parameters.

## 5. Conclusions

In this paper, the effects of different contents of Sb or Sr modification combined with T6 heat treatment on the microstructure and thermal and electrical conductivities of Al-8Si alloy were investigated. For Al-8Si alloy, the eutectic silicon aggregates when the alloy is modified by 0.3 wt.% or 0.5 wt.% Sb, which reduces the thermal and electrical conductivities of the alloy. Sb modification combined with T6 heat treatment or Sr modification can increase the thermal and electrical conductivities. Combined with T6 treatment, 0.5 wt.% Sb modification results in the fracture of long flake eutectic silicon, and the thermal and electrical conductivities of the alloy are 41.4% IACS, 175.0 W/(m·K), respectively. However, the eutectic silicon of Al-8Si modified by 0.12 wt.% Sr is fine fibrous, and the thermal and electrical conductivities of the alloy can reach 45.4% IACS, 193.7 W/(m·K), respectively, which decrease slightly to 45% IACS and 190.7 W/(m·K) after T6 heat treatment. Because even if the long flake eutectic silicon is broken or the fine eutectic silicon is spheroidized after T6 heat treatment, its size is still larger than that of fibrous eutectic silicon, and the electron scattering is correspondingly enhanced, so the enhancement of thermal and electrical conductivities is limited. The research in this article can provide a reference for improving the thermal and electrical conductivities by adjusting the microstructure of the hypoeutectic Al-Si alloy.

**Author Contributions:** Conceptualization, J.G. and J.-G.W.; methodology, J.G., J.-G.W. and Z.-P.G.; software, J.G. and Z.-P.G.; validation, J.G., R.-F.Y. and P.-K.M.; investigation, J.G., M.-H.W. and P.Z.; writing—original draft preparation, J.G.; writing—review and editing, J.G., J.-G.W. and Z.-P.G.; supervision, J.-G.W.; project administration, J.-G.W. and Z.-P.G.; funding acquisition, J.-G.W. All authors have read and agreed to the published version of the manuscript.

**Funding:** This research was funded by the National Key Research and Development Program of China (Grant Nos. 2018YFB2001801 and 2019YFB2006501) and the Science and Technology Development Program of Jilin Province (Grant No. 20190302059GX).

**Conflicts of Interest:** The authors declare no conflict of interest.

## References

1. Abdollahi, A.; Gruzleski, J.E. An evaluation of calcium as a eutectic modifier in A357 alloy. *Int. J. Cast Met. Res.* **1998**, *11*, 145–155. [[CrossRef](#)]
2. Cui, X.; Cui, H.; Wu, Y.; Liu, X. The improvement of electrical conductivity of hypoeutectic Al-Si alloys achieved by composite melt treatment. *J. Alloy. Compd.* **2019**, *788*, 1322–1328. [[CrossRef](#)]
3. Li, K.; Li, W.; Zhang, G.; Zhu, W.; Zheng, F.; Zhang, D.; Wang, M. Effects of Si phase refinement on the plasma electrolytic oxidation of eutectic Al-Si alloy. *J. Alloy. Compd.* **2019**, *790*, 650–656. [[CrossRef](#)]
4. Shaji, M.C.; Ravikumar, K.K.; Ravi, M.; Sukumaran, K. Development of a high strength cast aluminium alloy for possible automotive applications. *Mater. Sci. Forum* **2013**, *765*, 54–58. [[CrossRef](#)]
5. Rauta, V.; Cingi, C.; Orkas, J. Effect of annealing and metallurgical treatments on thermal conductivity of aluminium alloys. *Int. J. Met.* **2016**, *10*, 157–171. [[CrossRef](#)]
6. Stadler, F.; Antrekowitsch, H.; Fragner, W.; Kaufmann, H.; Pinatel, E.R.; Uggowitzner, P.J. The effect of main alloying elements on the physical properties of Al-Si foundry alloys. *Mater. Sci. Eng. A* **2013**, *560*, 481–491. [[CrossRef](#)]
7. Cui, X.; Wu, Y.; Liu, X.; Zhao, Q.; Zhang, G. Effects of grain refinement and boron treatment on electrical conductivity and mechanical properties of AA1070 aluminum. *Mater. Des.* **2015**, *86*, 397–403. [[CrossRef](#)]
8. Cui, X.; Wu, Y.; Zhang, G.; Liu, Y.; Liu, X. Study on the improvement of electrical conductivity and mechanical properties of low alloying electrical aluminum alloys. *Compos. Part B Eng.* **2017**, *110*, 381–387. [[CrossRef](#)]
9. Khaliq, A.; Rhamdhani, M.A.; Brooks, G.A.; Grandfield, J.F. Removal of vanadium from molten aluminum—Part II. Kinetic analysis and mechanism of VB<sub>2</sub> formation. *Metall. Mater. Trans. B* **2014**, *45*, 769–783. [[CrossRef](#)]
10. Cui, X.; Wu, Y.; Cui, H.; Zhang, G.; Zhou, B.; Liu, X. The improvement of boron treatment efficiency and electrical conductivity of AA1070Al achieved by trace Ti assistant. *J. Alloy. Compd.* **2018**, *735*, 62–67. [[CrossRef](#)]
11. Mulazimoglu, M.H.; Drew, R.A.L.; Gruzleski, J.E. Electrical conductivity of aluminium-rich Al-Si-Mg alloys. *J. Mater. Sci. Lett.* **1989**, *8*, 297–300. [[CrossRef](#)]
12. Mulazimoglu, M.H.; Drew, R.A.L.; Gruzleski, J.E. The electrical conductivity of cast Al-Si alloys in the range 2 to 12.6 wt pct silicon. *Metall. Trans. A* **1989**, *20*, 383–389. [[CrossRef](#)]
13. Narayan Prabhu, K.; Ravishankar, B.N. Effect of modification melt treatment on casting/chill interfacial heat transfer and electrical conductivity of Al-13% Si alloy. *Mater. Sci. Eng. A* **2003**, *360*, 293–298. [[CrossRef](#)]
14. Lumley, R.N.; Polmear, I.J.; Groot, H.; Ferrier, J. Thermal characteristics of heat-treated aluminum high-pressure die-castings. *Scripta Materialia* **2008**, *58*, 1006–1009. [[CrossRef](#)]
15. Choi, S.W.; Cho, H.S.; Kang, C.S.; Kumai, S. Precipitation dependence of thermal properties for Al-Si-Mg-Cu-(Ti) alloy with various heat treatment. *J. Alloy. Compd.* **2015**, *647*, 1091–1097. [[CrossRef](#)]
16. Lados, D.A.; Apelian, D.; Wang, L. Solution treatment effects on microstructure and mechanical properties of Al-(1 to 13 pct)Si-Mg cast alloys. *Metall. Mater. Trans. B* **2010**, *42*, 171–180. [[CrossRef](#)]
17. Vandersluis, E.; Ravindran, C. Effects of solution heat treatment time on the as-quenched microstructure, hardness and electrical conductivity of B319 aluminum alloy. *J. Alloy. Compd.* **2020**, *838*. [[CrossRef](#)]
18. Tiedje, N.S.; Taylor, J.A.; Easton, M.A. A new multi-zone model for porosity distribution in Al-Si alloy castings. *Acta Mater.* **2013**, *61*, 3037–3049. [[CrossRef](#)]
19. Barrirero, J.; Li, J.; Engstler, M.; Ghafoor, N.; Schumacher, P.; Odén, M.; Mücklich, F. Cluster formation at the Si/liquid interface in Sr and Na modified Al-Si alloys. *Scripta Mater.* **2016**, *117*, 16–19. [[CrossRef](#)]

20. Li, J.H.; Wang, X.D.; Ludwig, T.H.; Tsunekawa, Y.; Arnberg, L.; Jiang, J.Z.; Schumacher, P. Modification of eutectic Si in Al–Si alloys with Eu addition. *Acta Mater.* **2015**, *84*, 153–163. [[CrossRef](#)]
21. Rao, J.; Zhang, J.; Liu, R.; Zheng, J.; Yin, D. Modification of eutectic Si and the microstructure in an Al-7Si alloy with barium addition. *Mater. Sci. Eng. A* **2018**, *728*, 72–79. [[CrossRef](#)]
22. Li, B.; Wang, H.; Jie, J.; Wei, Z. Effects of yttrium and heat treatment on the microstructure and tensile properties of Al–7.5 Si–0.5 Mg alloy. *Mater. Des.* **2011**, *32*, 1617–1622. [[CrossRef](#)]
23. Farahany, S.; Ourdjini, A.; Idarsi, M.H.; Shabestari, S.G. Evaluation of the effect of Bi, Sb, Sr and cooling condition on eutectic phases in an Al–Si–Cu alloy (ADC12) by in situ thermal analysis. *Thermochimica Acta* **2013**, *559*, 59–68. [[CrossRef](#)]
24. Darlapudi, A.; McDonald, S.D.; Terzi, S.; Prasad, A.; Felberbaum, M.; StJohn, D.H. The influence of ternary alloying elements on the Al–Si eutectic microstructure and the Si morphology. *J. Cryst. Growth* **2016**, *433*, 63–73. [[CrossRef](#)]
25. Olafsson, P.; Sandstrom, R.; Karlsson, Å. Comparison of experimental, calculated and observed values for electrical and thermal conductivity of aluminium alloys. *J. Mater. Sci.* **1997**, *32*, 4383–4390. [[CrossRef](#)]
26. Lumley, R.N.; Deeva, N.; Larsen, R.; Gembarovic, J.; Freeman, J. The role of alloy composition and T7 heat treatment in enhancing thermal conductivity of aluminum high pressure diecastings. *Metall. Mater. Trans. A Phys. Metall. Mater. Sci.* **2013**, *44*, 1074–1086. [[CrossRef](#)]
27. Cho, Y.H.; Kim, H.W.; Lee, J.M.; Kim, M.S. A new approach to the design of a low Si-added Al–Si casting alloy for optimising thermal conductivity and fluidity. *J. Mater. Sci.* **2015**, *50*, 7271–7281. [[CrossRef](#)]
28. Vandersluis, E.; Lombardi, A.; Ravindran, C.; Bois-Brochu, A.; Chiesa, F.; MacKay, R. Factors influencing thermal conductivity and mechanical properties in 319 Al alloy cylinder heads. *Mater. Sci. Eng. A* **2015**, *648*, 401–411. [[CrossRef](#)]
29. Dinnis, C.M.; Taylor, J.A.; Dahle, A.K. As-cast morphology of iron-intermetallics in Al–Si foundry alloys. *Scripta Materialia* **2005**, *53*, 955–958. [[CrossRef](#)]
30. Faraji, M.; Katgerman, L. Distribution of trace elements in a modified and grain refined aluminium–silicon hypoeutectic alloy. *Micron* **2010**, *41*, 554–559. [[CrossRef](#)]
31. Simensen, C.J.; Nielsen, Ø.; Hillion, F.; Voje, J. NanoSIMS Analysis of trace element segregation during the Al–Si eutectic reaction. *Metall. Mater. Trans. A* **2007**, *38*, 1448–1451. [[CrossRef](#)]
32. Lu, S.Z.; Hellawell, A. The mechanism of silicon modification in aluminum–silicon alloys: Impurity induced twinning. *Metall. Trans. A* **1987**, *18*, 1721–1733. [[CrossRef](#)]
33. Nogita, K.; Yasuda, H.; Yoshida, K.; Uesugi, K.; Takeuchi, A.; Suzuki, Y.; Dahle, A.K. Determination of strontium segregation in modified hypoeutectic Al–Si alloy by micro X-ray fluorescence analysis. *Scripta Materialia* **2006**, *55*, 787–790. [[CrossRef](#)]
34. Nogita, K.; Yasuda, H.; Yoshiya, M.; McDonald, S.D.; Uesugi, K.; Takeuchi, A.; Suzuki, Y. The role of trace element segregation in the eutectic modification of hypoeutectic Al–Si alloys. *J. Alloy. Compd.* **2010**, *489*, 415–420. [[CrossRef](#)]
35. Lu, S.-Z.; Hellawell, A. Growth mechanisms of silicon in Al–Si alloys. *J. Cryst. Growth* **1985**, *73*, 316–328. [[CrossRef](#)]
36. Hansen, S.C.; Loper, C.R. Effect of antimony on the phase equilibrium of binary Al–Si alloys. *Calphad* **2000**, *24*, 339–352. [[CrossRef](#)]
37. Xiufang, B.; Weimin, W.; Jingyu, Q. Liquid structure of Al–12.5% Si alloy modified by antimony. *Mater. Charact.* **2001**, *46*, 25–29. [[CrossRef](#)]
38. Gustafsson, G.; Thorvaldsson, T.; Dunlop, G.L. The influence of Fe and Cr on the microstructure of cast Al–Si–Mg alloys. *Metall. Trans. A* **1986**, *17*, 45–52. [[CrossRef](#)]
39. Mohamed, A.M.A.; Samuel, A.M.; Samuel, F.H.; Doty, H.W. Influence of additives on the microstructure and tensile properties of near-eutectic Al–10.8%Si cast alloy. *Mater. Des.* **2009**, *30*, 3943–3957. [[CrossRef](#)]
40. Zhao, Q.; Qian, Z.; Cui, X.; Wu, Y.; Liu, X. Optimizing microstructures of dilute Al–Fe–Si alloys designed with enhanced electrical conductivity and tensile strength. *J. Alloy. Compd.* **2015**, *650*, 768–776. [[CrossRef](#)]
41. Hou, J.P.; Li, R.; Wang, Q.; Yu, H.Y.; Zhang, Z.J.; Chen, Q.Y.; Ma, H.; Wu, X.M.; Li, X.W.; Zhang, Z.F.; et al. Breaking the trade-off relation of strength and electrical conductivity in pure Al wire by controlling texture and grain boundary. *J. Alloy. Compd.* **2018**, *769*, 96–109. [[CrossRef](#)]

42. Karabay, S. Modification of AA-6201 alloy for manufacturing of high conductivity and extra high conductivity wires with property of high tensile stress after artificial aging heat treatment for all-aluminium alloy conductors. *Mater. Des.* **2006**, *27*, 821–832. [[CrossRef](#)]

**Publisher's Note:** MDPI stays neutral with regard to jurisdictional claims in published maps and institutional affiliations.



© 2020 by the authors. Licensee MDPI, Basel, Switzerland. This article is an open access article distributed under the terms and conditions of the Creative Commons Attribution (CC BY) license (<http://creativecommons.org/licenses/by/4.0/>).